J Mater Sci: Mater Electron (2016) 27:3873–3879
DOI 10.1007/s10854-015-4236-0

Influence of carbon atmosphere on surface morphology and photocatalytic activity of TiO_2 coatings by multi-heat treatment

Sujun Guan[1] · Liang Hao[2] · Hiroyuki Yoshida[3] · Hiroshi Asanuma[1] · Fusheng Pan[4] · Yun Lu[1]

Received: 15 October 2015 / Accepted: 14 December 2015 / Published online: 22 December 2015

Abstract Photocatalyst titanium dioxide (TiO_2) coatings on alumina (Al_2O_3) balls had been prepared by mechanical coating technique with titanium (Ti) powder and multi-heat treatment (pretreatment-oxidation–reduction). The influence of carbon atmosphere during multi-heat treatment on the surface structure and photocatalytic activity of TiO_2 coatings was investigated and characterized. Results show that thin coatings of TiO_2 and Ti_2CO form on the surface of Ti coatings during pretreatment in air or in carbon atmosphere, respectively. Due to the pretreatment, different surface morphologies of rutile TiO_2 form on the surface of Ti coatings, during subsequent oxidation in air. Oxygen vacancies are generated in the lattice of rutile TiO_2, during subsequent reduction in carbon atmosphere. The photocatalytic activity of the TiO_2 coatings prepared by multi-heat treatment is effectively enhanced, compared with the TiO_2 coatings prepared by solo-oxidation of Ti coatings. The visible light photocatalytic activity of TiO_2 coatings treated in carbon atmosphere could be effectively enhanced by more than eight times. The photocatalytic activity under ultraviolet is more related with nano-fiber morphology, while the photocatalytic activity under visible light is related with the narrowed band gap.

✉ Yun Lu
luyun@faculty.chiba-u.jp

[1] Graduate School and Faculty of Engineering, Chiba University, 1-33, Yayoi-cho, Inage-ku, Chiba 263-8522, Japan

[2] College of Mechanical Engineering, Tianjin University of Science and Technology, No. 1038, Dagu Nanlu, Hexi District, Tianjin 300222, People's Republic of China

[3] Chiba Industrial Technology Research Institute, 889, Kasori-cho, Wakaba-ku, Chiba 264-0017, Japan

[4] College of Materials Science and Engineering, Chongqing University, No. 174 Shazhengjie, Shapingba, Chongqing 400044, People's Republic of China

1 Introduction

Titanium dioxide (TiO_2) has been attracted much attention for numerous environmentally friendly applications in various fields, such as water and air purification, decontamination, the production of carbonaceous solar fuels, and the self-cleaning surfaces, due to its suitable band edge positions, excellent stability, and low cost [1–6]. However, the application of TiO_2 has been limited to the ultraviolet (UV) range due to its wider band gap, and fast electron–hole recombination due to a high density of trap stats [6–8]. Several reviews highlight the advances in the field of enhancing the visible-light active TiO_2 photocatalysts, mainly by sensitization with small band gap semiconductors, and narrowing the band gap via elemental doping [9–13]. Recently, it has been shown that manipulating structure morphology and electronic structure are an effective approaches to improve the separation and transportation of charge carriers [14–16]. An enormous amount of research has been devoted to introduction of oxygen vacancy into TiO_2. Oxygen vacancies could serve as shallow donors to form the extra electron energy levels to narrow the band gap [17, 18]. After Chen et al. reported the preparation of "black" anatase TiO_2, many researches have successively proven that hydrogen treatment is an effective method to form surface oxygen defects and enhance its photocatalytic activity [6, 19, 20]. As the problem of hydrogen treatment requires high-pressure hydrogen atmosphere, simpler and safer methods are expected to enhance the photocatalytic activity [21, 22].

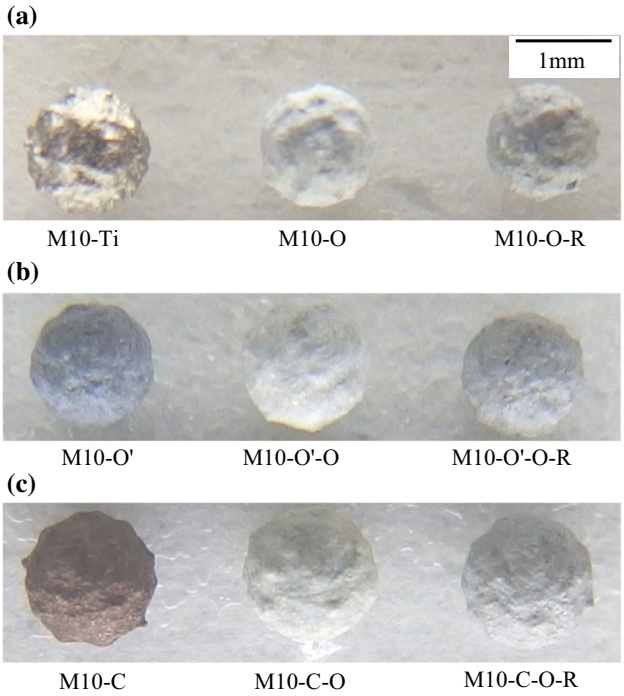

Fig. 1 Appearance photograph of the samples by multi-heat treatment. **a** Without pretreatment, **b** with pretreatment in air, **c** with pretreatment in carbon atmosphere

In this work, photocatalyst TiO_2 coatings were prepared by mechanical coating technique (MCT) and multi-heat treatment (pretreatment-oxidation–reduction). The influence of carbon atmosphere on the microstructure and photocatalytic activity of TiO_2 coatings was investigated and characterized. The relationship among photocatalytic activity and surface morphology as well as narrowed band gap is discussed.

2 Experimental

2.1 Preparation of Ti coatings

Ti powder (average diameter of 30 μm) and alumina (Al_2O_3) balls (average diameter of 1 mm) were used as the coating materials and the substrates, respectively. A planetary ball mill (Type: P6, Fritsch, Germany) was used to perform the mechanical coating operation. Ti coatings were fabricated by MCT, with the rotation speed of 480 rpm for 10 h, named as "M10-Ti". The detailed MCT procedure can be found in our previous works [23, 24].

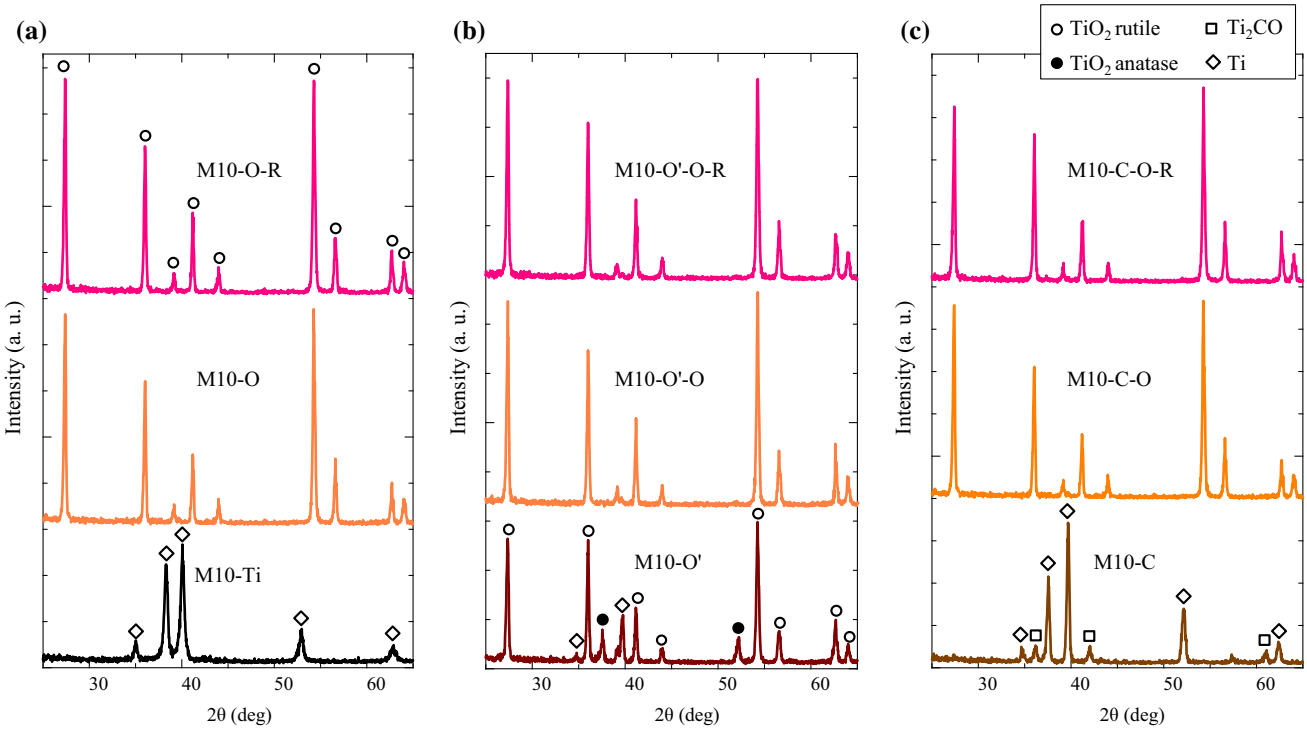

Fig. 2 XRD patterns of the samples by multi-heat treatment. **a** Without pretreatment, **b** with pretreatment in air, **c** with pretreatment in carbon atmosphere

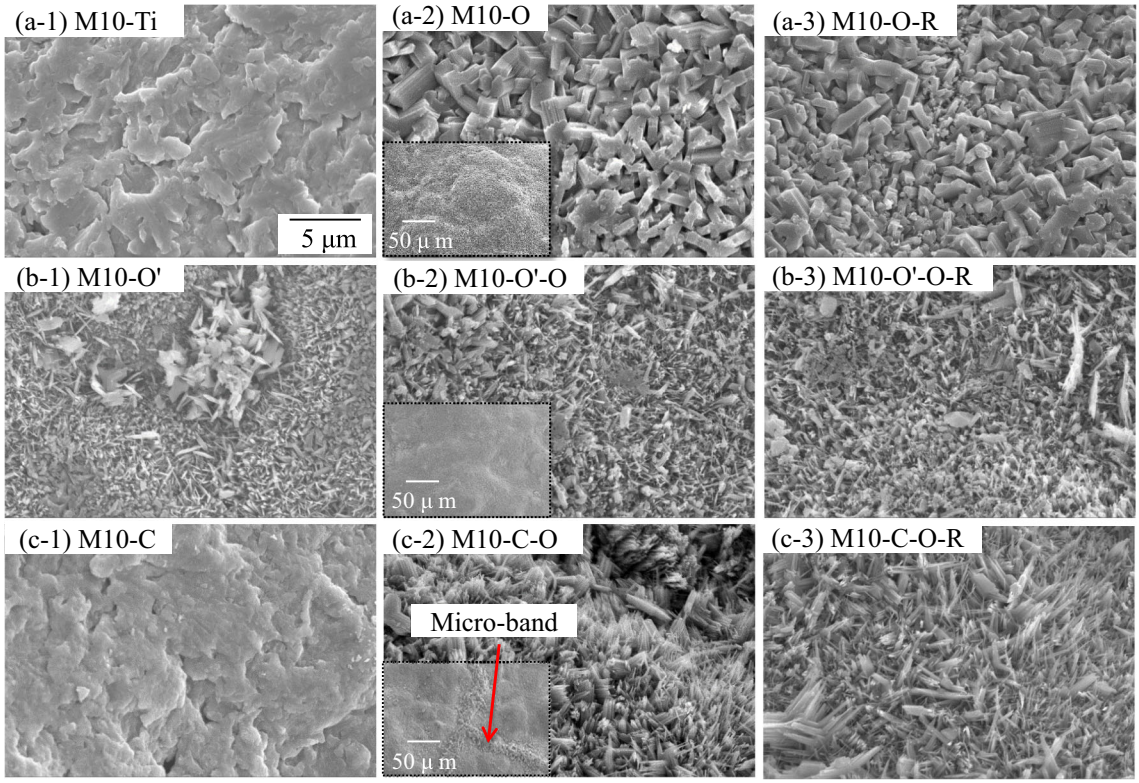

Fig. 3 Comparison of morphology of samples by multi-heat treatment. **a** Without pretreatment, **b** with pretreatment in air, **c** with pretreatment in carbon atmosphere

2.2 Preparation of photocatalyst coatings

The prepared Ti coatings were pretreated with carbon atmosphere (in carbon powder, average diameter of 150 μm) at 1073 K for 2 h, and named as "M10-C". The process of pretreatment with carbon atmosphere has been described in detail previously [25]. For comparison, the Ti coatings were also pretreated in air 1073 K for 2 h, named as "M10-O′". Then, the pretreated samples were oxidized at 1073 K for 15 h in air, named as "M10-C-O" and "M10-O′-O", respectively. Finally, the oxidized samples were treated in carbon atmosphere at 973 K for 0.5 h, named as "M10-C-O-R" and "M10-O′-O-R", respectively. In this work, the treatment in carbon atmosphere after oxidation is referred to as reduction.

2.3 Characterization

The crystal structure and phase purity of the prepared samples were analyzed by X-ray diffraction (XRD) (JDX-3530, JEOL, Japan) equipped with Cu-Kα radiation at 30 kV and 20 mA, employing a scanning rate of 0.02° s^{-1} in the range from 23° to 65°. The surface morphology and cross-sectional structure of the samples were observed by scanning electron microscopy (SEM) (JSM-5300, JEOL, Japan). The ultraviolet–visible absorption spectra of the prepared samples was measured by an ultraviolet–visible spectrophotometer (UV–Vis, Model MSV-370, Jasco, Japan) with a wavelength range of 370–750 nm.

2.4 Photocatalytic activity

Photocatalytic activity was evaluated by measuring the degradation rate of methylene blue (MB) solution (C_0: 10 μmol/L, 35 mL) under UV and visible light irradiation at room temperature by referring to Japanese Industrial Standard (JIS R 1703-2), which had been described in detail previously [24, 25]. The prepared samples were firstly dried under UV light (FL20S BLB, Toshiba) for 24 h, and adsorption of MB solution (20 μmol/L, 35 mL) was carried out in the dark for 18 h. The evaluation of photocatalytic activity was carried out under UV (irradiance of 1 w/cm^2, FL20S BLB, Toshiba) and visible light (irradiance of 5000 lux, NEC FL20SSW/18). To clearly show the photocatalytic activity of samples, the difference (Δk) of the degradation rate constants between k_{sample} and $k_{\text{MB solution}}$ was used.

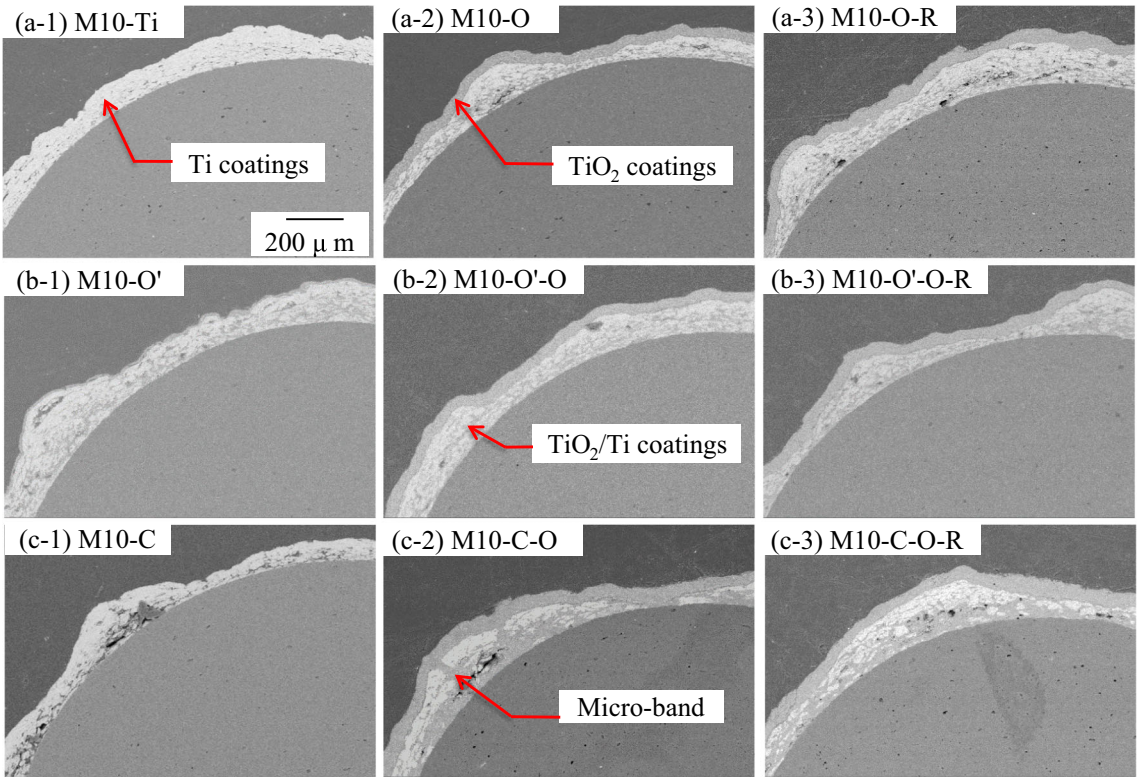

Fig. 4 Comparison of cross section of samples by multi-heat treatment. **a** Without pretreatment, **b** with pretreatment in air, **c** with pretreatment in carbon atmosphere

3 Results and discussion

3.1 Appearance and phase structure

From Fig. 1, it clearly shows the influence of carbon atmosphere on the appearance of the samples, during the multi-heat treatment. Without pretreatment, the color changes from silvery (M10-Ti) to light-white (M10-O) during oxidation, then to light-grey (M10-O-R) during reduction. With pretreatment in air, the color changes to dark-blue (M10-O′), then to dark-white (M10-O′-O) during oxidation, then to dark-grey (M10-O′-O-R) during reduction. While with pretreatment in carbon atmosphere, the color changes to brown (M10-C), then to dark-white with slight yellow (M10-C-O) during oxidation, then to grey (M10-C-O-R) during reduction.

Figure 2 shows the XRD patterns of the samples during the multi-heat treatment. With pretreatment in air, the relatively higher diffraction peaks of rutile TiO_2 and lower peaks of anatase TiO_2 are detected from the M10-O′ sample, indicating that TiO_2 is formed on the surface of Ti coatings. While with pretreatment in carbon atmosphere, the diffraction peaks at 36.1°, 42.0°, and 60.9° could be attributed to the (111), (200), and (220) crystal planes of Ti_2CO, respectively. After oxidation in air, the diffraction peaks of samples are well indexed to the crystal planes of rutile TiO_2, indicating that only rutile TiO_2 is formed. During subsequent reduction in carbon atmosphere, there is no evident change in the formed phases.

Considering the appearance and XRD patterns, the color becomes dark-blue (M10-O′) after pretreatment in air is related to the formation of TiO_2 with mixed-phase of anatase and rutile on the surface (Fig. 2b). The color becomes brown (M10-C) during pretreatment in carbon atmosphere, which is related to the formation of the phase Ti_2CO on the surface (Fig. 2c). The difference in color during subsequent oxidation among M10-O, M10-O′-O and M10-C-O is related to surface morphology and thickness of the crystal coatings [23–25]. The color change during reduction indicates that reduction affects the formation of oxygen vacancies, which produce the color centers of Ti^{3+} in the TiO_2 [26, 27], and this is similar to these results obtained by hydrogen treatment [7, 20].

3.2 Microstructure evolution

After subsequent oxidation, the effect of pretreatment in air or carbon atmosphere on the surface morphology is shown in Fig. 3. Compared with M10-O sample, the crystal size of the samples with two kinds of pretreatment (M10-O′-O and

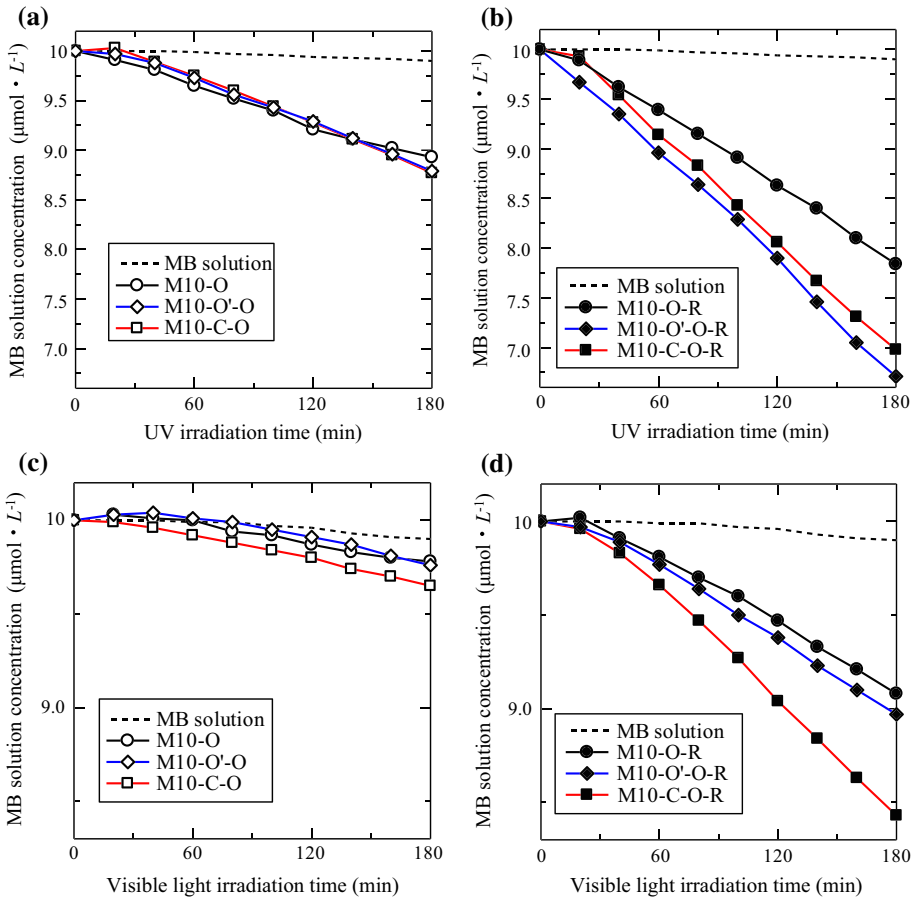

Fig. 5 Comparison of the photocatalytic activity towards the degradation of MB solution. **a**, **b** Under UV irradiation, **c**, **d** under visible light irradiation

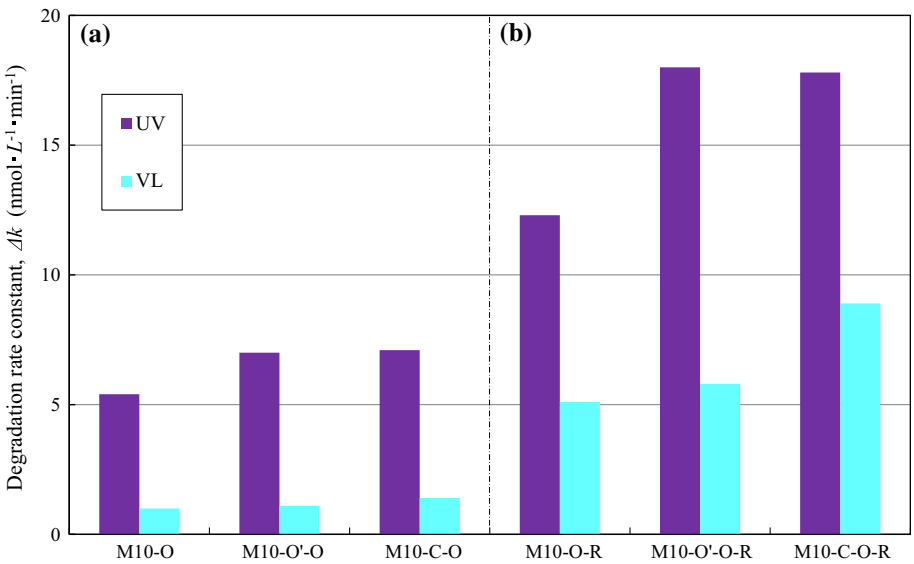

Fig. 6 Comparison of the degradation rate constant of samples. **a** The samples after oxidation, **b** the samples after reduction

M10-C-O) is smaller and the surface morphology changes from columnar (M10-O) to micro-size (M10-O′-O) and nano-fiber (M10-C-O), especially along micro-bands (M10-C-O) [25]. Micro-bands are clearly observed on the surface of M10-C-O sample, but not on the other two samples (M10-O and M10-O′-O). Moreover, after further reduction in carbon powder, the change of surface morphology is slight.

Morphology change shows that the formed TiO_2 and Ti_2CO during pretreatment in air and carbon atmosphere

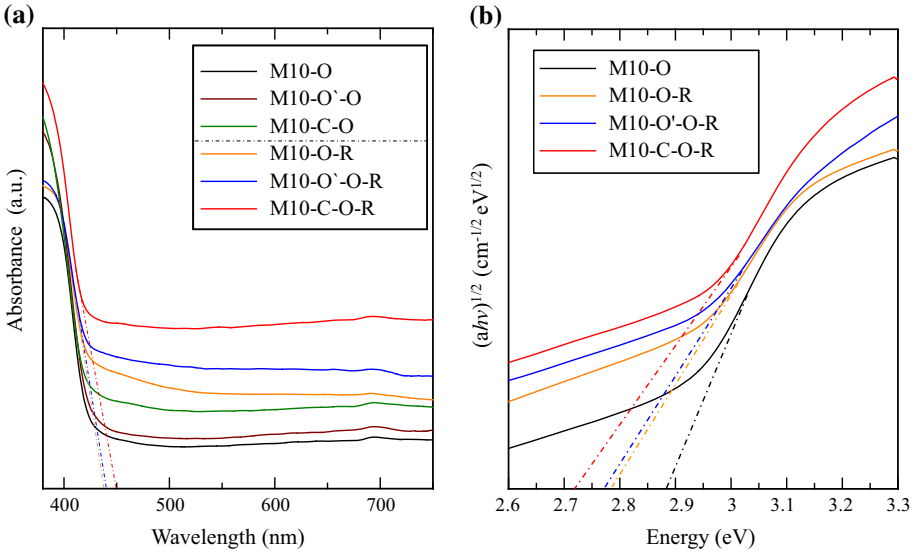

Fig. 7 **a** UV–Vis absorption spectra of the as-prepared samples, **b** plots of $(ahv)^{1/2}$ versus the photon energy (hv) of the UV–Vis absorption spectra

respectively, have a remarkable effect on the subsequent oxidation process. It is well known that Ti can easily react with oxygen to form titanium oxide, and the growth of titanium oxide depends on the predominant diffusion of Ti or oxygen [28, 29]. The predominance diffusion of Ti versus oxygen is influenced by oxygen concentration, oxidation temperature, and the initial layer on the surface of Ti coatings [30]. Various morphologies of titanium oxide, such as pin-shaped, lamellar and needle, or nanofiber, could be formed during different oxidation processes [29–31]. Compared with the M10-O sample, the morphology change on the sample of M10-O′-O and M10-C-O is due to the initial coatings of TiO_2 and Ti_2CO formed during pretreatment, could cause the oxidation process to occur under a different low oxygen concentration [32, 33]. Therefore, the pretreatment is the main factor on the morphology change, which causes the different growth model of TiO_2 during the subsequent oxidation.

Figure 4 shows SEM images of the change of cross sections of the samples, during multi-heat treatment. While pretreatment in air, the TiO_2 coatings could be found from M10-O′ and the thickness is about 5 μm, while Ti_2CO formed during pretreatment in carbon atmosphere is too thin to be detected from M10-C. During subsequent oxidation, the different initial oxidized coatings could affect the oxygen concentration, which is matched with the change of surface morphology. After oxidation, the thickness of oxidized samples is similar, while more inner layer had been oxidized (M10-C-O). The more inner oxidized layer is related with the micro-crack formed during pretreatment in carbon atmosphere [25]. Moreover, after reduction, the cross sections of the samples hardly change.

3.3 Photocatalytic activity

The photocatalytic activity of as-prepared samples is evaluated by degradation of MB solution under UV and visible light irradiation, as shown in Fig. 5. For all samples, the concentration of MB solution decreased at different rates under UV and visible light irradiation. It means all samples show photocatalytic activity. After oxidation, the effect on photocatalytic activity of pretreatment in carbon atmosphere is obvious under visible light irradiation (Fig. 5c). After reduction, the influence of carbon atmosphere for all samples is significant, as shown in Fig. 5b, d. Compared with pretreatment, the enhancement on photocatalytic activity of carbon atmosphere under visible light irradiation (Fig. 5d) is more significant than that of under UV irradiation (Fig. 5b).

Figure 6 shows the degradation rate constants Δk of MB solution with different samples. It can be seen that pretreatment effect on photocatalytic activity under UV irradiation is similar, while pretreatment effect in carbon atmosphere on photocatalytic activity under visible light irradiation is more effective than that of pretreatment in air. Compared with the TiO_2 coatings prepared by solo-oxidation of Ti coatings, the visible light photocatalytic activity of TiO_2 coatings treated in carbon atmosphere by multi-heat treatment could be effectively enhanced by more than eight times.

The influence of carbon atmosphere on photocatalytic activity could be attributed to the following reasons. Oxygen vacancies generated in the lattice of TiO_2 coatings during reduction is the main factor to shift absorption to the visible light region, as shown in Fig. 7a. The shifted visible

light absorption benefits the narrowed band gap from 2.88 eV of M10-O sample to 2.78 eV of M10-C-O-R sample (Fig. 7b), to generate more photo-induced electrons and holes to enhance the photocatalytic activity [34–36]. In addition, the pretreatment effect of carbon atmosphere on surface morphology is another factor to further enhance the reduction effect, as shown by the photocatalytic activity (Fig. 5b, d). It could be concluded that the photocatalytic activity under UV is more related with surface morphology, while the photocatalytic activity under visible light is related with the narrowed band gap.

4 Conclusions

In summary, we have demonstrated that the multi-heat treatment with carbon atmosphere is a safe, simple, and effective strategy to enhance the photocatalytic activity of TiO_2 coatings. The formed oxide coatings during pretreatment benefit the formation of TiO_2 coatings with smaller surface morphology during subsequent oxidation. Oxygen vacancies generated in the lattice of TiO_2 coatings during the reduction is in favor of shifting the visible light absorption, which effectively enhances the photocatalytic activity under UV and visible light irradiation. The smaller surface morphology further enhances the reduction effect. The photocatalytic activity under ultraviolet (UV) is more related with surface morphology, while the photocatalytic activity under visible light is related with the narrowed band gap.

Acknowledgments This work is supported by the National Nature Science Foundation of China (No. 51404170).

References

1. S. Kumar, L. Devi, J. Phys. Chem. A **115**, 13211–13241 (2011)
2. A. Fujishima, X. Zhang, D.A. Tryk, Surf. Sci. Rep. **63**, 515–582 (2008)
3. H. Wang, T. Wang, P. Xu, J. Mater. Sci. Mater. Electron. **9**, 327–330 (1998)
4. L. Liu, H. Zhao, J. Andino, Y. Li, ACS Catal. **2**, 1817–1828 (2012)
5. K. Prabakaran, S. Mohanty, S. Nayak, J. Mater. Sci. Mater. Electron. **25**, 4590–4602 (2014)
6. G. Wang, H. Wang, Y. Ling, Y. Tang, X. Yang, R. Fitzmoris, C. Wang, J. Zhang, Y. Li, Nano Lett. **11**, 3026–3033 (2011)
7. X. Ma, X. Ni, J. Mater. Sci. Mater. Electron. **26**, 1129–1135 (2015)
8. Y. Li, J. Zhang, Laser Photonics Rev. **4**, 517–528 (2010)
9. R. Daghrir, P. Drogui, D. Robert, Ind. Eng. Chem. Res. **52**, 3581–3599 (2013)
10. L. Pan, J. Zou, X. Zhang, L. Wang, Ind. Eng. Chem. Res. **49**, 8526–8531 (2010)
11. M. Ni, M. Leung, D. Leung, K. Sumathy, Renew. Sustain. Energy Rev. **11**, 401–425 (2007)
12. G. Wang, X. Yang, F. Qian, J. Zhang, Y. Li, Nano Lett. **10**, 1088–1092 (2010)
13. J. Lim, P. Murugan, N. Lakshminarasimhan, J. Kim, J. Lee, S. Lee, W. Choi, J. Catal. **310**, 91–99 (2014)
14. F. Taleshi, J. Mater. Sci. Mater. Electron. **26**, 3262–3267 (2015)
15. H. Song, S. You, T. Chen, X. Jia, J. Mater. Sci. Mater. Electron. **26**, 8442–8450 (2015)
16. D. Potapenko, Z. Li, J. Kysar, R. Osgood, Nano Lett. **14**, 6185–6189 (2014)
17. M. Setvin, U. Aschauer, P. Scheiber, Y. Li, W. Hou, M. Schmid, A. Selloni, U. Diebold, Science **341**, 988–991 (2013)
18. I. Grinberg, D.V. West, M. Torres, G. Gou, D.M. Stein, L. Wu, G. Chen, E.M. Gallo, A.R. Akbashev, P.K. Davies, J.E. Spanier, A.M. Rappe, Nature **503**, 509–512 (2013)
19. X. Chen, L. Liu, P. Yu, S. Mao, Science **331**, 746–750 (2011)
20. X. Yu, B. Kim, Y. Kim, ACS Catal. **3**, 2479–2486 (2013)
21. Z. Wang, C. Yang, T. Lin, H. Yin, P. Chen, D. Wan, F. Xu, F. Huang, J. Lin, X. Xie, M. Jiang, Energy Environ. Sci. **6**, 3007–3014 (2013)
22. S. Yang, W. Tang, Y. Ishikawa, Q. Feng, Mater. Res. Bull. **46**, 531–537 (2011)
23. Y. Lu, S. Guan, L. Hao, H. Yoshida, Coatings **5**, 425–464 (2015)
24. Y. Lu, K. Kobayashi, S. Guan, L. Hao, H. Yoshida, H. Asanuma, J. Chen, Mater. Sci. Semicond. Process. **30**, 128–134 (2015)
25. S. Guan, L. Hao, Y. Lu, H. Yoshida, F. Pan, H. Asanuma, Mater. Sci. Semicond. Process. **41**, 358–363 (2015)
26. S. Hoang, S. Guo, N. Hahn, A. Bard, C. Mullins, Nano Lett. **12**, 26–32 (2012)
27. X. Lu, G. Wang, T. Zhai, M. Yu, J. Gan, Y. Tong, Y. Li, Nano Lett. **12**, 1690–1696 (2012)
28. G. Mor, O. Varghese, M. Paulose, K. Shankar, C. Grimes, Sol. Energy Mater. Sol. Cells **90**, 2011–2075 (2006)
29. X. Peng, A. Chen, J. Mater. Chem. **14**, 2542–2548 (2004)
30. F. Gracia, J. Holgado, L. Contreras, T. Girardeau, A. Gonzalez-Elipe, Thin Solid Films **429**, 84–90 (2003)
31. M. Thamima, S. Karuppuchamy, J. Mater. Sci. Mater. Electron. (2015). doi:10.1007/s.10854-015-3774-9
32. U. Diebold, Surf. Sci. Rep. **48**, 53–229 (2003)
33. N. Birks, G.H. Meier, F.S. Pettit, *Introduction to the High-Temperature Oxidation of Metals* (Cameridge University Press, Cameridge, 2006)
34. H. Yaghoubi, Z. Li, Y. Chen, H. Ngo, V. Bhethanabotla, B. Joseph, S. Ma, R. Schlaf, A. Takshi, ACS Catal. **5**, 327–335 (2015)
35. X. Bai, L. Wang, R. Zong, Y. Lv, Y. Sun, Y. Zhu, Langmuir **29**, 3097–3105 (2013)
36. H. Tan, Z. Zhao, W. Zhu, E. Coker, B. Li, M. Zheng, W. Yu, H. Fan, Z. Sun, ACS Appl. Mater. Interfaces **6**, 19184–19190 (2014)